A mixed strain rate and energy based fatigue criterion for short fiber reinforced thermoplastics

I. Raphael, N. Saintier, H. Rolland, G. Robert, L. Laiarinandrasana

Version of Record: https://www.sciencedirect.com/science/article/pii/S014211231930235X
Manuscript_568490de2683709da96e2d5beae11963

A mixed strain rate and energy based fatigue criterion for short fiber reinforced thermoplastics

I. Raphael[a,b], N. Saintier[a,*], H. Rolland[a], G. Robert[b], L. Laiarinandrasana[c]

[a] *I2M, Arts et Métiers ParisTech, Esplanade des Arts et Métiers, 33405 Talence, France*
[b] *Solvay Performance Polyamides, Avenue Ramboz, BP 64, 69192 Saint-Fons, France*
[c] *PSL Research University, MINES ParisTech, Centre des Matériaux, CNRS UMR 7633, BP 87, 91003 Evry, France*

Abstract

Multiple parameters influence the durability of reinforced thermoplastics under fatigue loading. Having models unifying as many of these parameters, while providing an accurate estimation of the fatigue lifetime, is thus key. This investigation on the evolution of multiple mechanical parameters under cyclic loading, and based on a large experimental database (more than 200 uniaxial fatigue tests over a wide range of load ratios), two cyclic strain-rate based criteria are proposed. The second is more elaborated, introducing anelastic energy, to better account for mean stress effect and unify fatigue life predictions within scatter bands of factor two.

Keywords: Thermoplastic; Short fiber composite; Fatigue criterion; Anisotropy; Mean stress effect;

1. Introduction

Reinforced thermoplastics are increasingly used in the industry as a light-weight solution to replace metallic parts. Parts made of short glass fiber reinforced polyamide are injection molded, which matches the high production rates of the automotive industry, even for parts with complex geometries. However the durability of these materials under fatigue loading still needs to be better understood and modeled in order to design and manufacture reliable parts.

A large number of parameters influences the durability of reinforced thermoplastics under fatigue loading [1], among which are: fibers geometry and orientation [2], loading frequency [3], mean stress [4], temperature, relative humidity [5], geometrical defects [6], etc. Relatively few studies have been dedicated to the mean stress effect [7]. Yet it has a major impact on the material behavior which exhibits significant visco-elasticity at ambient temperature that may in turn have a strong effect on its durability. When addressing the mean stress effect two approaches are possible. The first one consists in the use of classical empirical models that explicitly embed a mean stress effect (eg. Goodman & Gerber equations [8, 9] including with modifications to account for cyclic creep of the material, Chaboche model [10]).

* *Email:* nicolas.saintier@ensam.eu

The second option is to investigate mechanical quantities that would embed the mean stress effect while unifying the overall fatigue data set. When considering a visco-elastic material under cyclic loading, cyclic creep may play an important role in the mean stress sensitivity as illustrated by some previous authors. Among them, Horst [2] studied a polyamide 6 reinforced with 30wt% short glass fibers and showed that a parameter based on the evolution of the cyclic creep speed (determined from the measurement of the global displacement rate in stage II) could unify fatigue results for two sets of specimens sampled at different positions on an injection molded plate. Mourglia-Seignobos [11] also showed that this parameter unifies results at different testing temperatures (25°C, 65°C, 140°C) on a polyamide 6.6 reinforced with 30wt% short glass fibers. Finally Bernasconi [3] showed that the cyclic strain rate unifies fatigue results for various loading frequencies (1-4 Hz), also on a polyamide 6.6 reinforced with 30wt% short glass fibers.

This approach closely resembles those for creep of thermoplastic specimens. Under a static imposed load, the creep speed can directly be related to the time to rupture using the Monkman-Grant relationship [12]. But while many studies have been performed on static creep (a time dependent phenomenon), not much data exists for cyclic creep (a cycle dependent phenomenon) during stress-controlled fatigue testing.

In this study, a large fatigue database was established and analyzed in order to study the evolution of multiple mechanical parameters including energy based quantities and cyclic creep. Based on such analyses we propose a fatigue criterion able to capture both the orientation and load ratio effects. First materials, specimens and testing conditions used in this study as well as the experimental procedure will be described. Then, experimental results are presented with an analysis of a wide range of mechanical parameters. Finally, two fatigue criteria based on the cyclic strain rate are proposed with the aim of unifying results for multiple fiber orientations and mean stress levels including negative load ratios.

2. Materials and methods

2.1. Materials

The material studied is a polyamide 6.6 reinforced with 30wt% short glass fibers. It is supplied by Solvay Performance Polyamides under the commercial name Technyl®A218V30. Specimens are machined rectangular plates obtained by injection moulding (fig. 1(a)). Nominal thickness of the plates is 3.24 mm. Exact dimensions of individual specimens are measured prior to testing. Injection molding induces a heterogeneous orientation of fibers in the thickness of the plates. This structure is usually described as a superposition of three layers: the skin, the shell and the core (Horst [2], Bernasconi [13], Arif [5], Ayadi [14] and Rolland [15]). In the shell, the thickest part (2.8 mm over a total thickness of 3.24 mm), fibers are aligned with the injection flow. Conversely, at the center of the plate, is a $300\mu m$ thick layer referred to as the core. In this layer, fibers are perpendicular to the injection flow. This orientation is caused by an extensional flow as the molten material enters the mold cavity.

Samples were cut following the three usual orientations compared to the main injection direction: 0°, 45°and 90°(fig. 1(b)). This was necessary in order to investigate the effect of the macroscopic anisotropy of the material on its durability.

Since the mechanical properties of the polyamide matrix are sensitive to its water uptake, the material relative humidity (RH) has to be stable before and during testing. Following the standard protocol used by Solvay research teams, specimens were put in an environmental chamber at 70°C, RH=62% of humidity until their water uptake stabilization. Then, they spent 15 days at 23°C, RH=50% to reach the desired equilibrium humidity content of 50% of relative humidity (RH50 specimens). After conditioning, specimens are sealed in individual packets to prevent any change in RH prior to the experiment.

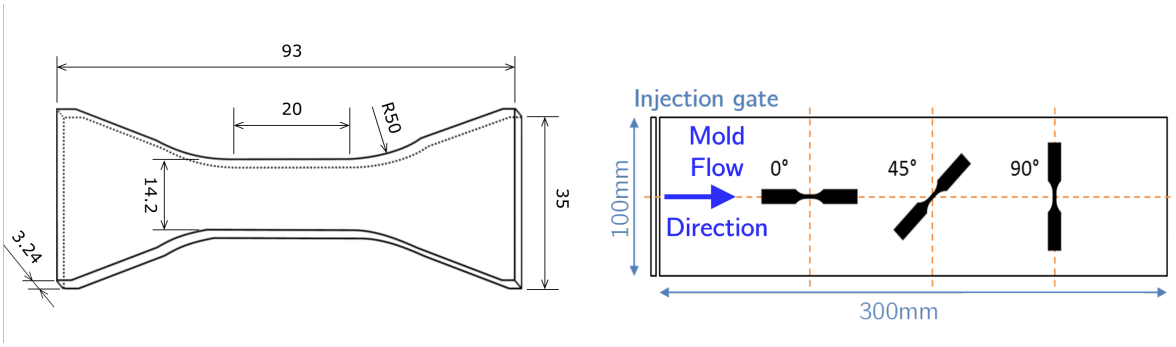

(a) Specimen geometry (b) Specimen orientation

Figure 1: Specimen geometry and orientation.

2.2. Methods

2.2.1. Mechanical testing

All testing was performed under load control, and strain evolution was monitored using and extensometer and digital image correlation (DIC). A clip on extensometer (class 0.5) with a gage length of 12mm was used. DIC strain field is averaged over the same zone monitored with the extensometer. DIC and extensometer were both used systematically, and DIC data was used when the extensometer knives moved during the test due to cyclic loading, making the extensometer data inaccurate.

Two fatigue machines were used in this study to perform uniaxial loading of the specimens.

First, a servo-hydraulic MTS fatigue machine was used at Solvay research laboratory. In this case air cooling of the specimen was used to prevent heating (indicated as *forced convection* in the results section). This machine was used to performed testing at multiple load ratios (R=-0.5 to R=0.7), for a total of 207 fatigue tests included in this work. A climate chamber allowed for the medium to be kept at a constant temperature (23°C ± 0.5°C) and humidity (50% RH). Testing was performed at a frequency of 3Hz.

Second, an electro-mechanical Bose Electroforce testing machine was used in the I2M laboratory for additional testing. Thanks to this "cold" technology, no air cooling was used in this case (indicated as *free convection* in the results section). This machine was only used to performed testing at R=0.1, for a total of 62 fatigue tests included in this work. Room temperature was controlled and kept at constant temperature (23°C ± 0.5°C) and humidity (50% RH) of the specimens was assumed constant during these

shorter tests. Testing was performed at a frequency of 3Hz for most of the specimens, only tests at higher stress levels were performed at 0.5Hz in order to limit self-heating. Those are clearly indicated on the data presented in the results section.

Surface temperature of the specimen was monitored using a FLIR thermal camera during testing. This allowed to insured a limited self-heating of the specimens.

2.2.2. Mechanical parameters

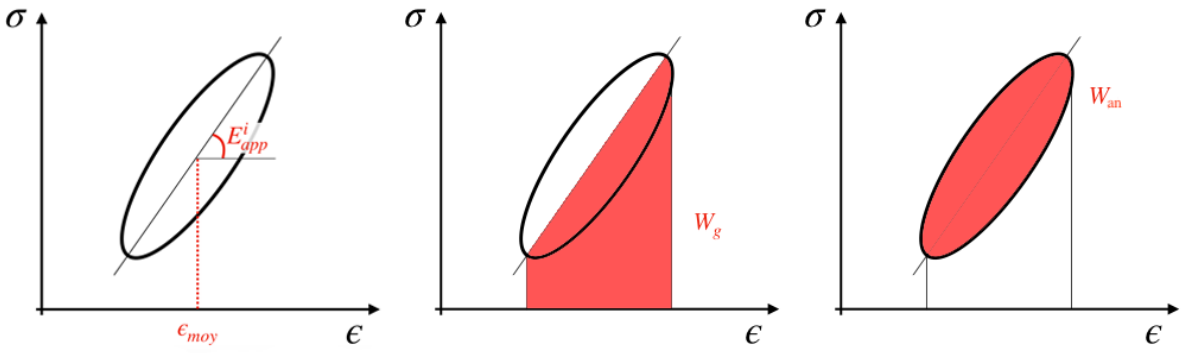

(a) Modulus and mean strain (b) Given strain energy W_g (c) Anelastic energy W_{an}

Figure 2: Mechanical parameters.

When considering a load cycle on a viscoelastic composite several mechanical quantities can be considered of interest for monitoring. In the present case of uniaxial loading, fig. 2 illustrates the chosen parameters:

- **the apparent modulus,** E_{app} (fig. 2(a)). For composite materials a decrease in the apparent modulus is often associated with the development of cyclic damage in the specimen. However it should be noticed that due to the visco-elastic behavior of the polyamide matrix the direct link between damage and modulus drop is not straight forward in our case. The apparent modulus at the i^{th} cycle, E^i_{app}, is calculated from the strain and stress amplitudes as:

$$E^i_{app} = \frac{\sigma^i_{max} - \sigma^i_{min}}{\epsilon^i_{max} - \epsilon^i_{min}} \tag{1}$$

- **given total strain energy density per cycle** W_g (fig. 2(b)). When considering multiaxial fatigue criteria the given elastic strain energy density is a parameter that is considered to efficiently describe multiaxial fatigue data by many authors [16]. As an energy parameter it is naturally sensitive to the mean stress effect (at constant stress amplitude the given strain energy increases as the mean stress increases).

  In our case since the purely elastic strain energy is difficult to address unambiguously (and independently of a model choice) the total given strain energy over a cycle is considered here and computed as follows:

$$W_g = \int_{cycle} < \sigma \dot{\epsilon}_t > \ \mathrm{d}t \tag{2}$$

where <> stands for the Macaulay brackets, σ the axial stress component and ϵ_t for the total axial strain component. The total given strain energy W_g is the amount of energy given to the material during loading.

W_g was experimentally determined as the area under the apparent modulus.

- **anelastic strain energy per cycle** W_{an} (fig. 2(c)). In a general thermodynamic framework, the hysteresis area results from the contribution of intrinsic dissipation, stored energy variation and thermomechanical coupling sources. For pure polyamide, Benaarbia *et al.* [17] have shown that the later are negligible for PA6.6 so that the anelastic strain energy density W_{an} per cycle can be written as follows:

$$W_{an} = \int_{cycle} \sigma \ \mathrm{d}\epsilon = W_s + D_i \tag{3}$$

Where W_s stands for the stored energy density per cycle and D_i for the intrinsic dissipation (that can be evaluated from thermal measurements under certain conditions, see [18]). It should be noticed that the balance between W_s and D_i is not constant over the whole fatigue life.

W_g was experimentally determined as the area of the hysteresis loop.

- **Axial mean strain** ϵ_{moy} (fig. 2(a)). The mean strain is calculated for every cycle and is classically associated with a ratcheting effect. Yet, for polymer materials, the evolution of this mean strain drift is generally considered as a so called cyclic creep rather than ratcheting that may be associated to different physical deformation mechanisms.

Note that stress and energy based quantities were evaluated from measured strain and nominal stress computations since accessing of true stress/strain values would need a full computational model considering the visco-elasto-plastic behavior of the material which is beyond the scope of this paper.

Moreover as only the axial strain is considered here, extension to notched specimens or multiaxial loadings might require the use of more appropriate parameters for strain (equivalent strain, maximal principal strain...) and energy measurements [19].

3. Experimental results

3.1. S-N curves

Fatigue test results are usually presented by plotting the imposed stress versus the number of cycles to failure, giving what is known as a S-N curve, or Wöhler curve. Figure 3 shows such S-N curves, plotted for the three fiber orientations at several load ratios. All stress values have been normalized by an arbitrary value for confidentiality reasons.

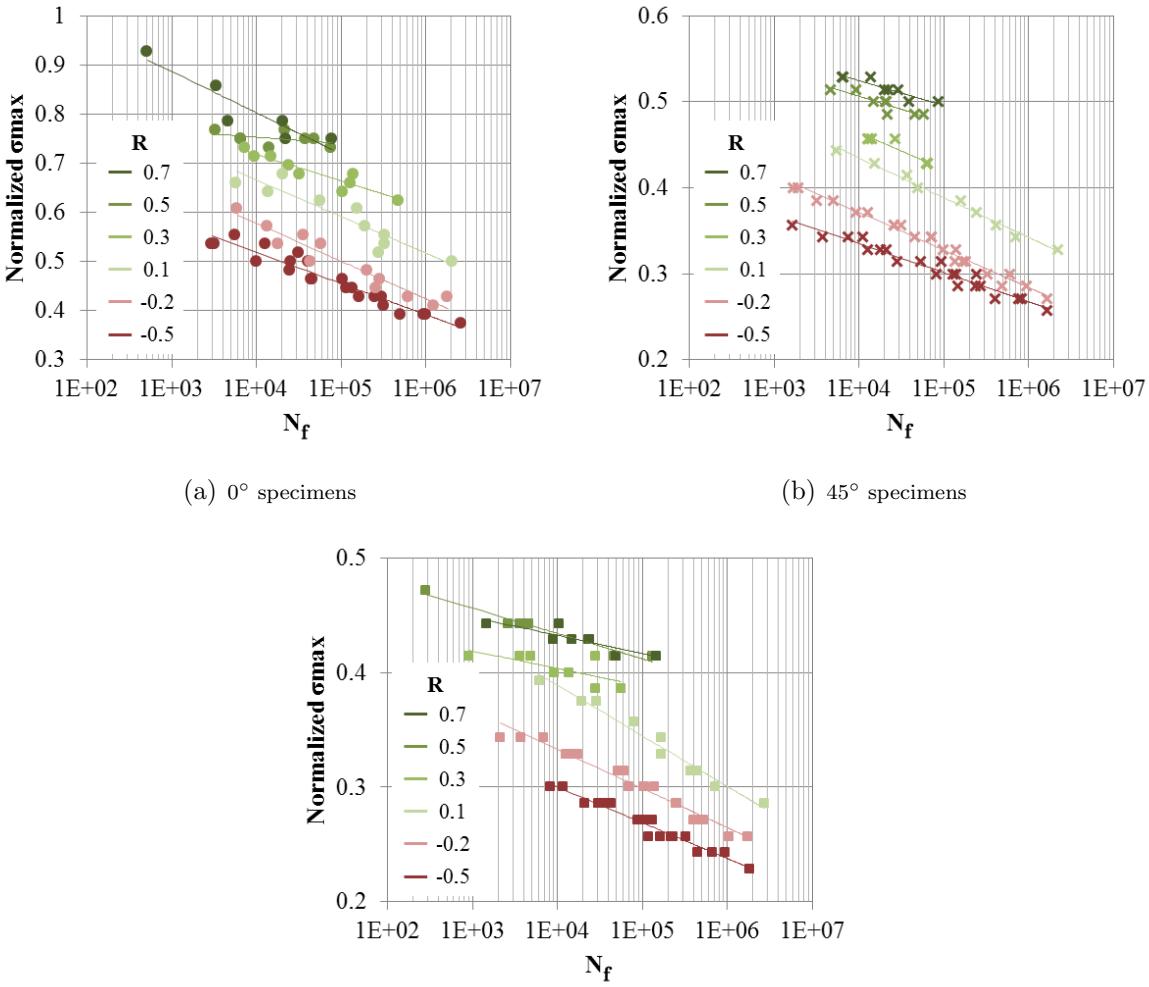

(a) 0° specimens

(b) 45° specimens

(c) 90° specimens

Figure 3: S-N curves - RH50 specimens - f = 3Hz - forced convection.

These first results show the strong influence of fiber orientation on the fatigue behavior of the material. For a given load ratio and a given applied stress, the number of cycles to failure is much greater if the fibers are mainly aligned with the loading (0° specimens). This is classically observed in the literature and the observed offsets in between different orientations are very similar to already published results (see [2, 20] for exemple). The load ratio has a strong impact: for a given mean stress, the lower the load ratio -which implies a higher stress amplitude- the lower the lifespan of the specimen (fig. 4).

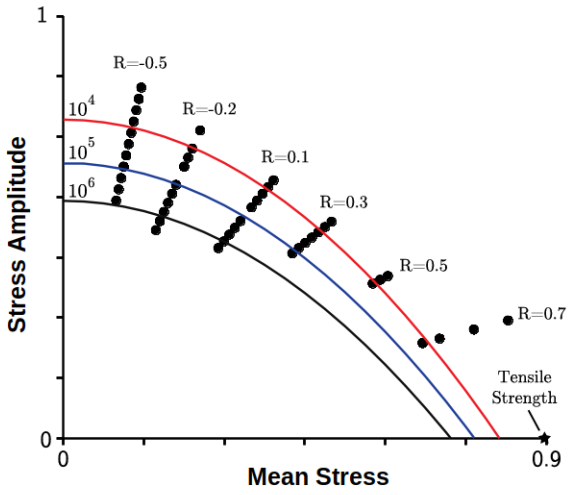

Figure 4: Normalized Haigh diagram for 0° specimens. Modified Gerber equations are plotted as proposed in the work of Mallick and Zhou [8] with adaptation for a 3Hz loading frequency - RH50 - f = 3Hz - forced convection.

3.2. Evolution of the mechanical parameters

3.2.1. Apparent modulus

Figure 5 illustrates the evolution of the moduli during fatigue testing for 0°, 45° and 90° specimens and for different fatigue lives. There is a very strong decrease in the modulus over the first 2000 cycles, for all lifetime ranges and the three orientations. For short tests ($N_f < 10^4$ cycles), the modulus drop is continuous from the beginning to the end of the test. For tests with lifetimes between 10^4 and 10^5 cycles, there is a difference in evolution depending on the orientation of the fibers. The moduli of the 90° specimens clearly stabilize after the first 2000 cycles until failure. The 45° specimens have moduli that change slope after the first 2000 cycles. Stable moduli are found in the case of long tests ($N_f > 10^5$ cycles) and slightly decreasing in the case of intermediate life tests. The 0° specimens have the largest modulus decrease without stabilization during testing, regardless of the lifetime range.

3.2.2. Energetic parameters

Given total strain energy density. The evolution of W_g for different fiber orientations and maximum stress levels is given in fig. 6. In all cases W_g stabilize after a few hundred (0°) to thousand cycles (45°, 90°). As the stress is imposed and constant, the increase is

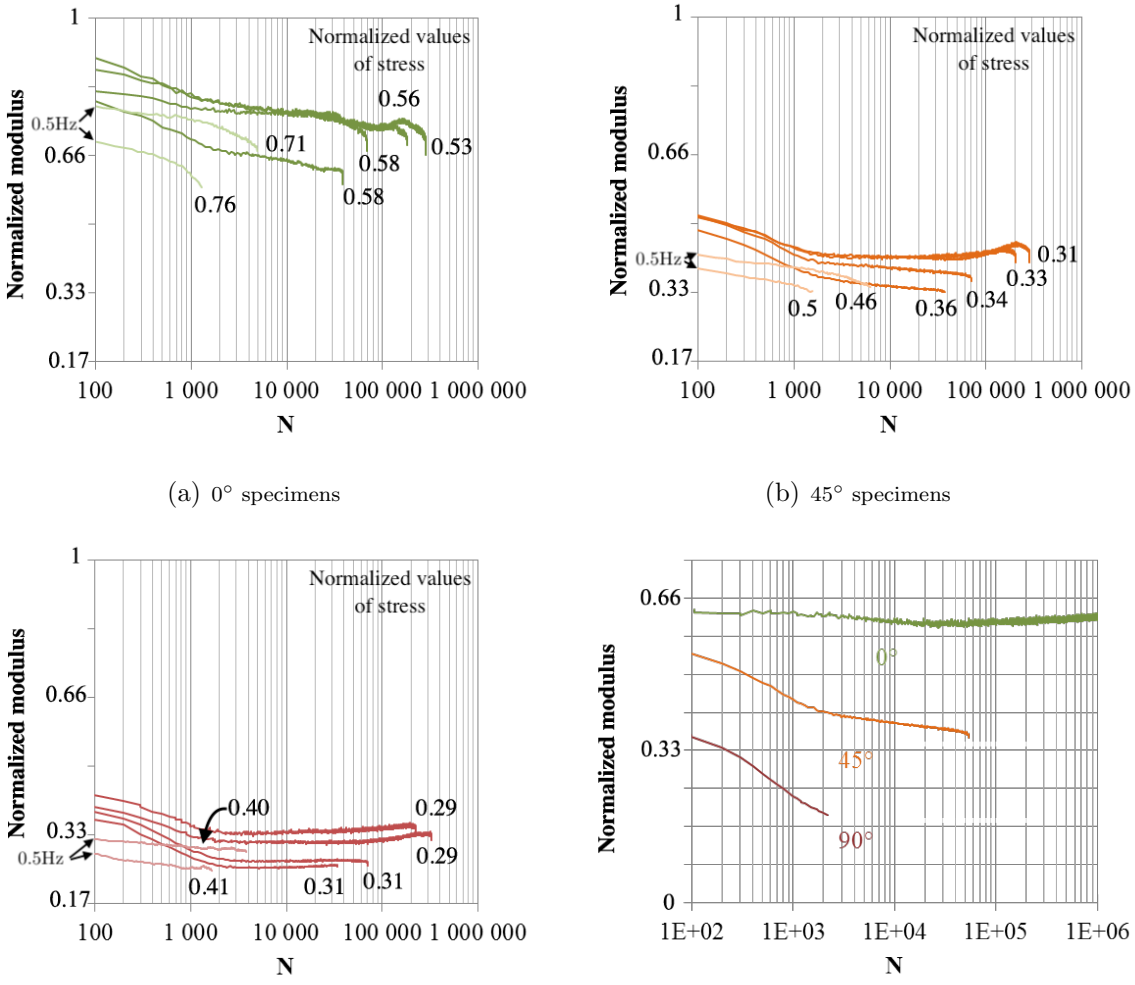

(a) 0° specimens

(b) 45° specimens

(c) 90° specimens

(d) Specimens submitted to the same stress, normalized $\sigma_{max} = 0.35$, and f=3Hz

Figure 5: Evolution of the apparent modulus - RH50 specimens - R=0.1 - f = 3Hz unless otherwise stated - free convection.

mostly due to an increase of the total strain amplitude associated with the softening effect induced by progressive damage and/or thermal softening. It should be noticed that this evolution is similar to the one observed for the apparent modulus. At equivalent fatigue lives, the amount of energy supplied is much higher for 0° specimens (fig. 6) compared to other orientations. Moreover when specimens are subjected to similar stress levels (same frequency, normalized $\sigma_{max} = 0.35$, see fig. 6(d)), W_g is almost stable for 0° specimens while there is a significant increase during the first 2000 cycles, then a stabilization until rupture for the 45° specimen. For the 90° specimen on fig. 6(d) testing at a high stress level and 3Hz led to significant self-heating and thus to a failure prior to stabilization.

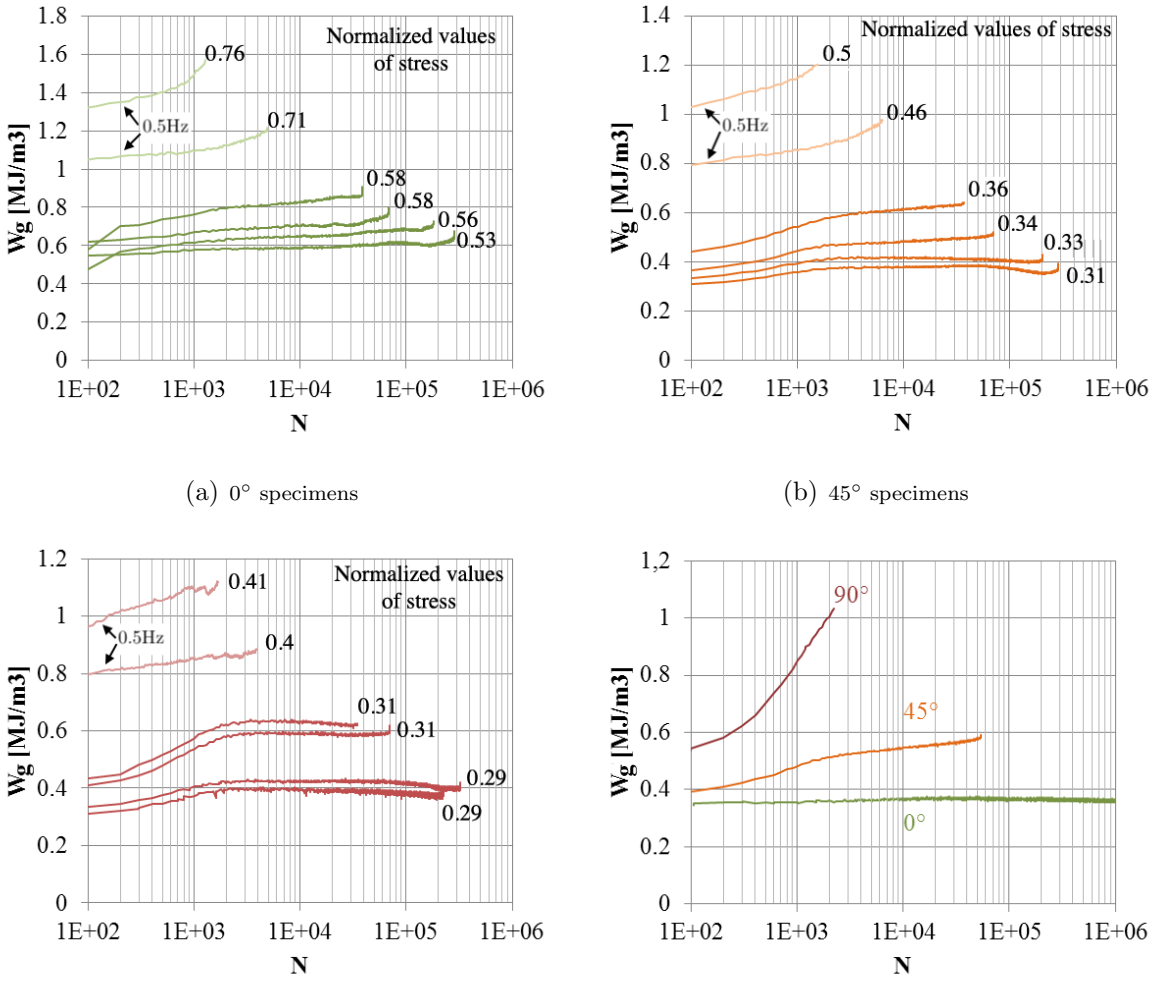

(a) 0° specimens

(b) 45° specimens

(c) 90° specimens

(d) Specimens submitted to the same stress, normalized $\sigma_{max} = 0.35$, and f=3Hz

Figure 6: Evolution of the given energy W_g - RH50 specimens - R=0.1 - f = 3Hz unless otherwise stated - free convection.

Figure 7 illustrates the evolution of this parameter for load ratios R ranging from -0.5 to 0.7, for all three fiber orientations and resulting in a lifetime close to 60,000 cycles. It can be seen that W_g is particularly stable during the test when the load ratio is high and

the slope increases for the lowest ratios (close to 0 and negative load ratios). It should be noted that at identical fatigue life, low stress ratios are associated with higher stress amplitudes as usually encountered. This change in the evolution of the W_g parameter corresponds to a change in the fatigue damage driving force for low and high load ratios as proposed in the following sections.

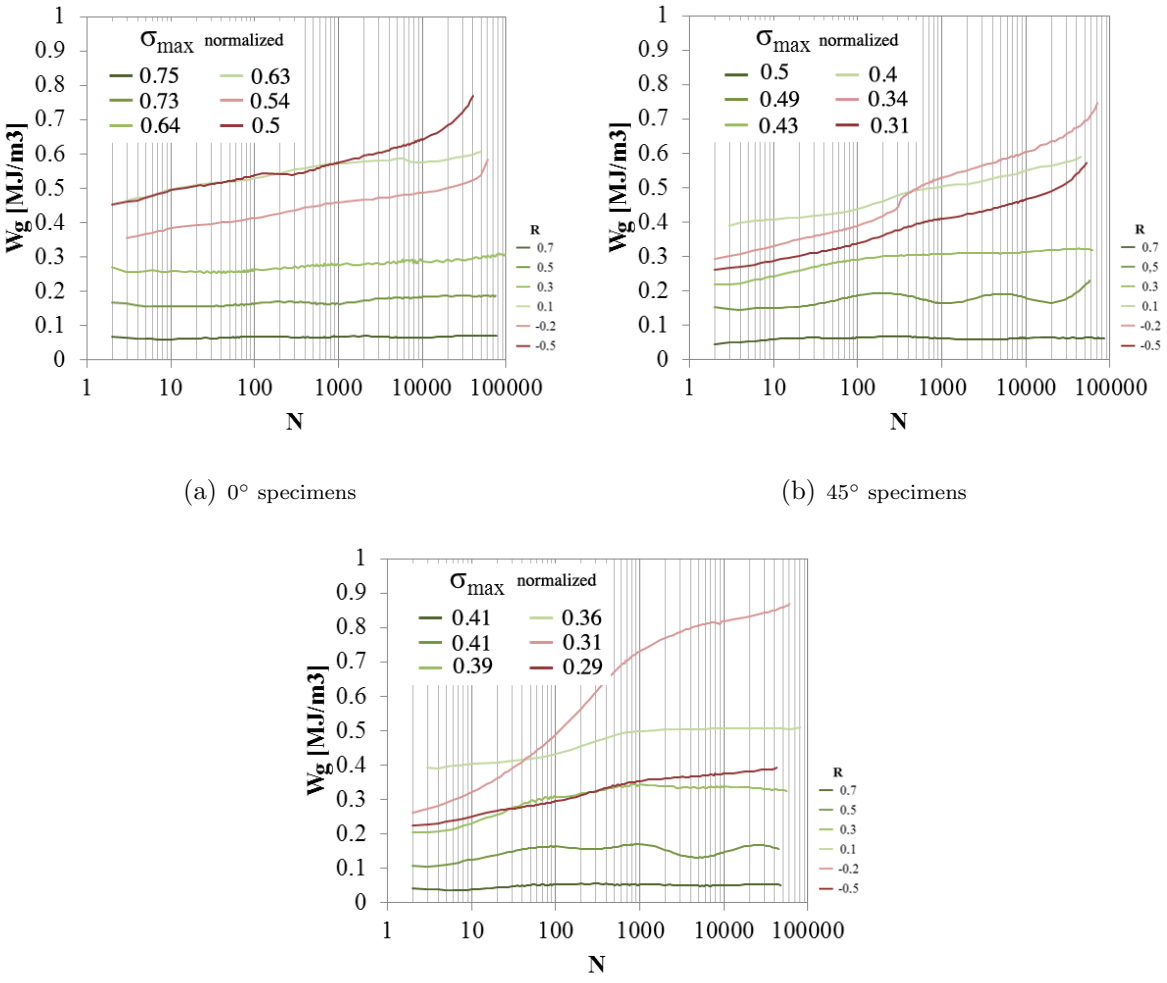

(a) 0° specimens

(b) 45° specimens

(c) 90° specimens

Figure 7: Evolution of the given energy W_g for different load ratios - RH50 specimens - f = 3Hz - forced convection.

Anelastic strain energy. The amount of anelastic energy is calculated for each recorded cycle to observe its evolution during the 3Hz fatigue tests (fig. 8). For similar lifespans, this quantity has the same order of magnitude regardless of orientation. Indeed, the values are relatively close and there is no clear hierarchy between the orientations.

The evolution of the anelastic energy during fatigue tests varies from one specimen to another. For 90° specimens it changes a little during the test and tends to decrease after a maximum is reached around 2000 cycles. This is also the case for low stress tests

for 0° specimens. In the case of the highest stresses for 45° and 0° specimens, the same sequence is observed: a high initial value that increases very rapidly after the first few hundred cycles until failure. Tests on 0° specimens conducted for longer fatigue lives have an anelastic energy amount that increases very slowly throughout the test. In the case of similar loads, the anelastic energy of the 0° specimen slowly decreases while that of the 90° specimen increases strongly.

In the case of tests with different load ratios (fig. 9), the anelastic energy values are close from one orientation to another but a marked hierarchy according to the load ratio R can be observed. The higher the R ratio, the lower the anelastic energy and the less the variation over the course of the test. In the case of negative ratios, this amount of energy is high and increases throughout the test, with faster evolution as the failure approaches.

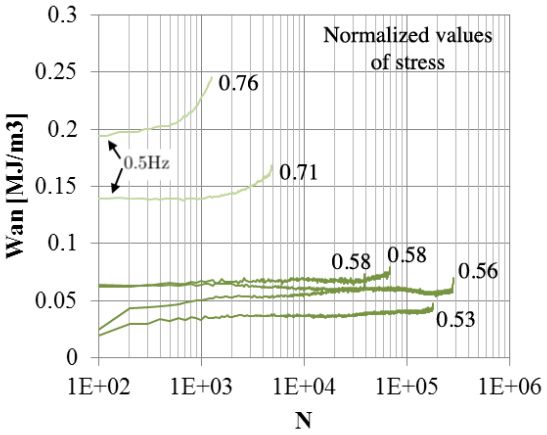

(a) 0° specimens

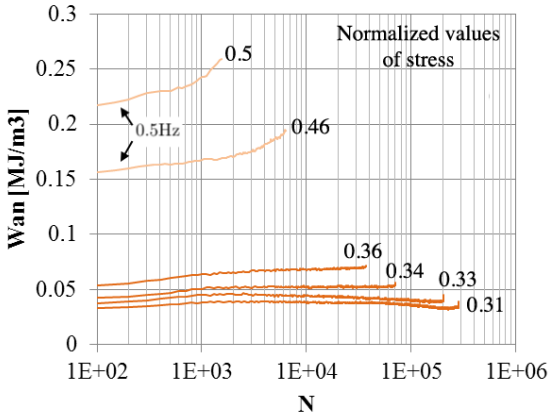

(b) 45° specimens

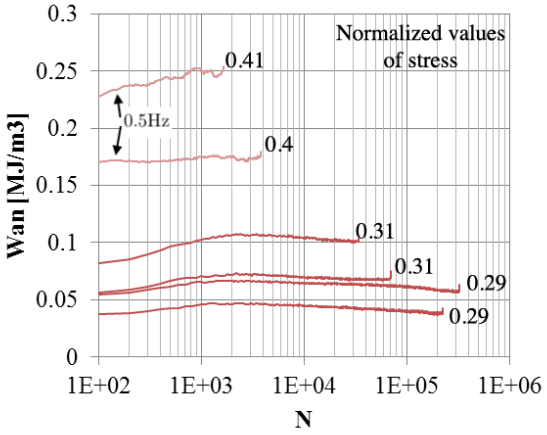

(c) 90° specimens

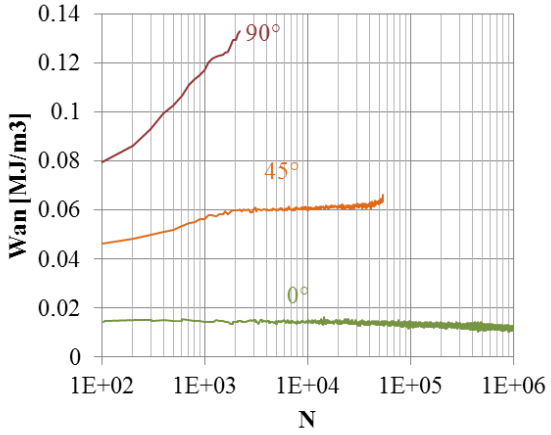

(d) Specimens submitted to the same stress, normalized $\sigma_{max} = 0.35$, and f=3Hz

Figure 8: Evolution of the anelastic energy W_{an} - RH50 specimens - R=0.1 - f = 3Hz unless otherwise stated - free convection.

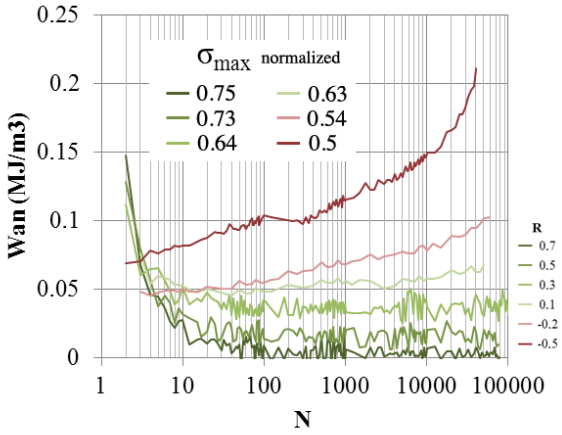

(a) 0° specimens

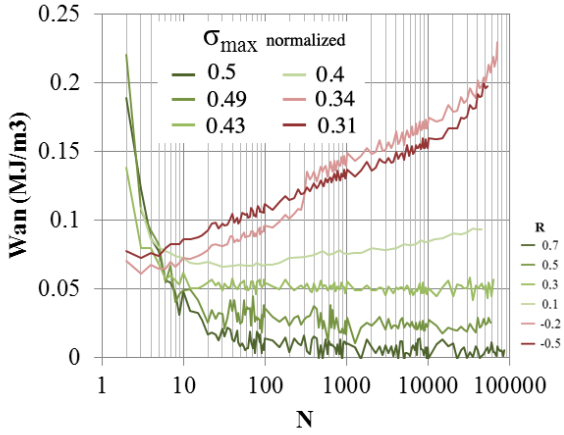

(b) 45° specimens

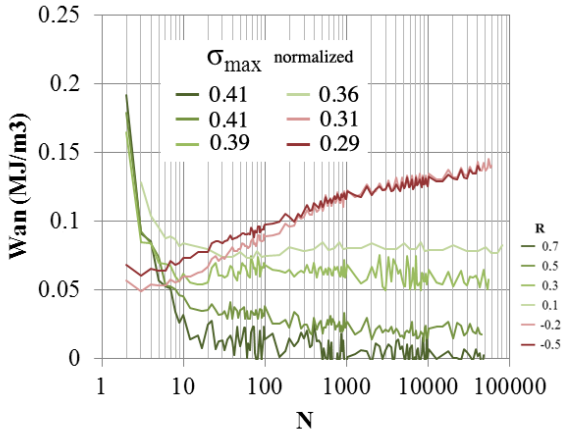

(c) 90° specimens

Figure 9: Evolution of the anelastic energy W_{an} for different load ratios - RH50 specimens - f = 3Hz - forced convection.

3.2.3. Mean strain

Figure 10 shows the evolution of the mean strain for the different lifetime ranges and for the three selected orientations for testing at R=0.1. It can be seen that in all cases, the mean strain increases throughout the test. This effect exists regardless of the lifetime range or fiber orientation. It should be noted that for a given lifetime, the hierarchy between the different orientations is always the same: the mean strain is greater for 90° specimens than for 45° specimens, which itself is higher than that of 0° specimens. It is worth noticing that the mean strain evolution is similar to the one observed during creep experiment but with a very limited (yet measurable) tertiary stage prior to failure. These aspect will be further discussed in subsection 4.1.

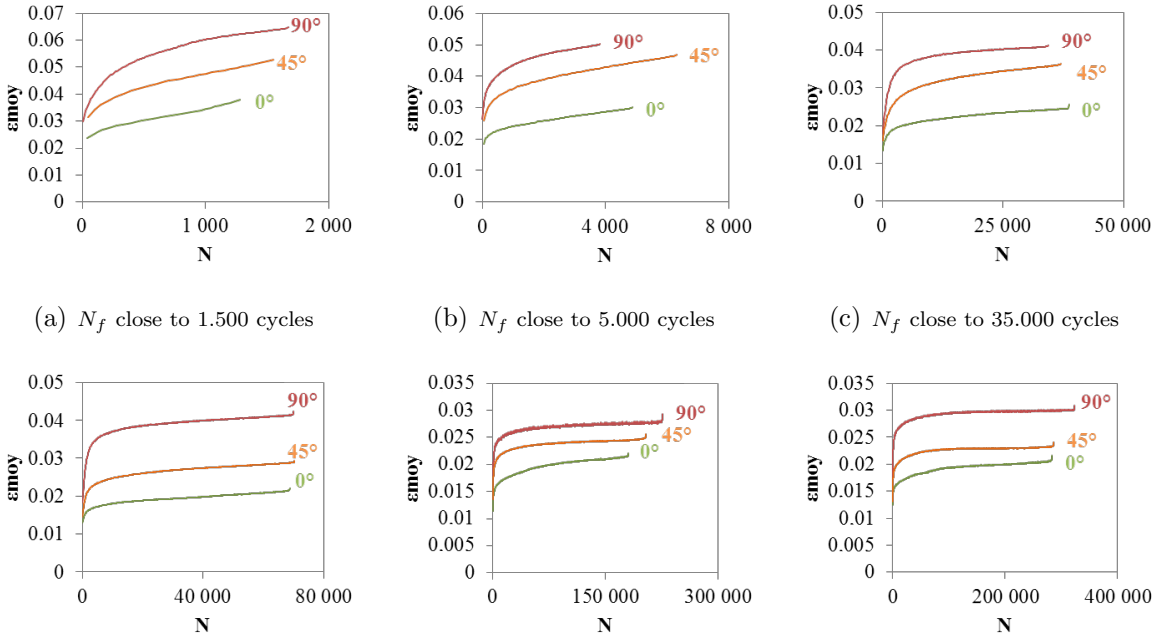

(a) N_f close to 1.500 cycles (b) N_f close to 5.000 cycles (c) N_f close to 35.000 cycles

(d) N_f close to 70.000 cycles (e) N_f close to 200.000 cycles (f) N_f close to 300.000 cycles

Figure 10: Evolution of the mean strain for several fatigue lives - RH50 specimens - R=0.1 - f = 3Hz - free convection.

Similar evolution of the mean strain can be observed at other load ratios, even for negative ones, as shown on fig. 11 (note that the abscissa is in logarithmic scale for this graph, to show the mean strain evolution for both low and high N_f).

4. Fatigue criterion

4.1. Relations between mechanical parameters and fatigue life

The objective is to propose a fatigue criterion that would be able to unify the fatigue data presented previously, independently of the fiber orientation and load ratio, with a limited number of parameters. As previously mentioned, traditional stress based S-N curves are not satisfactory to estimate a lifetime for different load ratios or fiber

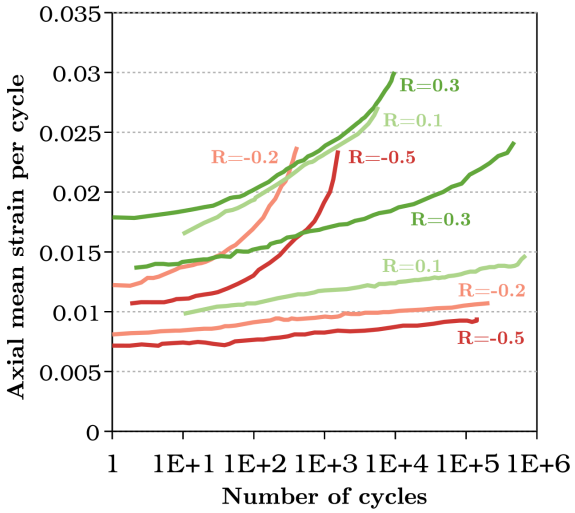

Figure 11: Evolution of the mean strain for several load ratios and fatigue lives - RH50 - f = 3Hz - forced convection.

orientations: for a given maximum stress value, the lifetime can vary from a few hundred to several million cycles depending on fiber orientation, load ratio or RH value. As testing is performed under load control, parameters based on the dual variable (i.e. the strain) should be studied in order to capture the material behavior. Choice should be made about which of the parameters presented above is best linked to the material lifetime and should thus be included in a fatigue criterion.

In the case of energy based parameters, it was chosen to consider the average value of these quantities over the entire test. In the case where the stabilization phase is rapid in relation to the total duration of the test, the choice of the value of the quantity at mid-life may also be relevant and was found to approximate well the mean value during the test.

Figure 12 illustrates the plot of the average values of W_g and W_{an} against the corresponding total fatigue lifetime for each test. It shows that both energetic parameters make it possible to better unify the fatigue test results than a stress based parameter and are able to take into account the orientation effects for tests with a load ratio below 0.3 for the given strain energy parameter and below 0.1 for the anelastic strain energy parameter. However for higher load ratio there is a significant offset of the Energy-N_f correlation. It should be noticed that if the slope of the anelastic strain energy W_{an} vs. N_f appears to be constant as R increases, the given strain energy parameter W_g vs. N_f trend seems to flatten as the load ratio increases which corresponds to a drop in the sensitivity of this parameter to the total fatigue lifetime.

As stated previously the axial mean strain does not stabilize during fatigue tests. Plotting the evolution of the mean strain versus the number of loading cycles N yields a curve similar to what would be obtained during a creep test (fig. 13(a)) - but with the variable N on the abscissa axis instead of the usual time t . It also has to be noticed that the creep level encountered in the cyclic tests is much higher than the one that would be obtained under a static creep test at the same maximum stress (as reported by

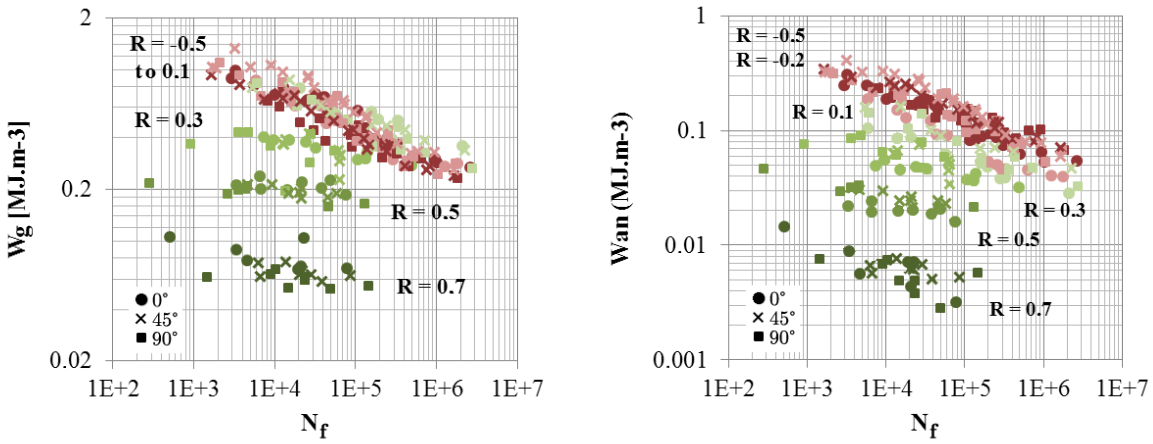

(a) Given energy vs. N_f

(b) Anelastic energy vs. N_f

Figure 12: Energetic values vs. N_f - RH50 specimens - f = 3Hz - forced convection.

Vinogradov [21]). By analogy to the measurement of the strain rate during secondary creep, the slope of the curve is measured at mid-life. This slope gives the cyclic strain rate (noted $\dot{\epsilon}_{cycl} = \frac{\partial \epsilon_{moy}}{\partial N}$) at mid-life.

Figure 13 shows the results obtained after such an analysis over the whole data base. By comparing fig. 12 and fig. 13 it is of clear evidence that the strain rate parameter unifies to a far greater extent the fatigue dataset independently of the load ratio and specimen orientation. Only fatigue tests at a load ratio of -0.5 and -0.2 seem to be less well captured by this parameter. Those tests correspond to fatigue tests with lower levels of applied axial mean stress.

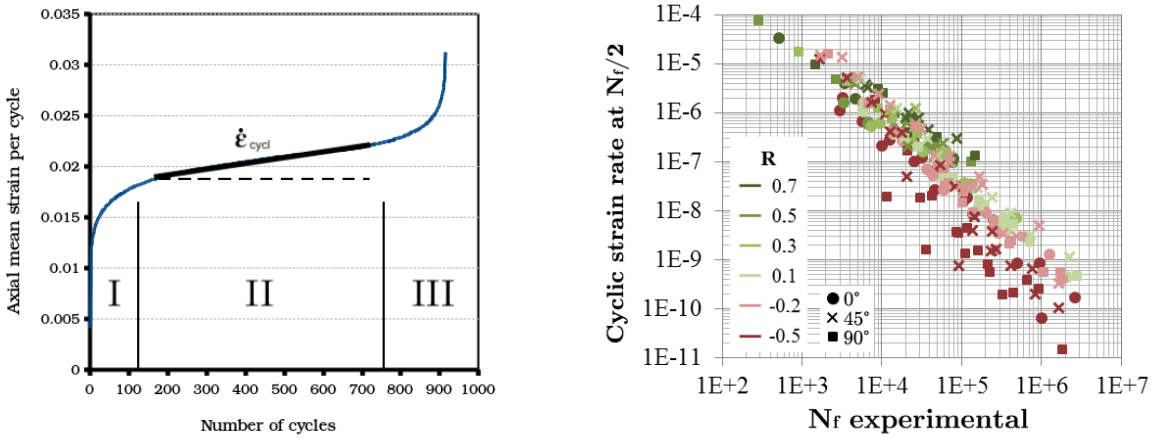

(a) Typical mean strain evolution

(b) Cyclic strain rate vs. N_f

Figure 13: Cyclic strain rate - RH50 specimens - f = 3Hz - forced convection.

4.2. Cyclic strain rate based criterion

In a first attempt, the lifetime was estimated from the cyclic strain rate $\dot{\epsilon}_{cycl}$ at mid fatigue life:

$$N_f = A \left(\frac{\dot{\epsilon}_{cycl}}{\dot{\epsilon}_0} \right)^n \tag{4}$$

with $\dot{\epsilon}_0 = 1s^{-1}$ to obtain a dimensionless indicator and the parameters A and n empirically evaluated from best fit of experimental results:

$A = 0.734$ and $n = -0.664$ for free convection tests.
$A = 0.631$ and $n = -0.638$ for forced convection tests.

The calculated lifetime is then compared with the one obtained experimentally (fig. 14). Figure 14(a) shows that the estimation of the lifetime by the cyclic-strain rate based criterion is very good for all three fiber orientations and loading frequencies at R=0.1. Moreover fig. 14(b) shows that the criterion unifies results for the different load ratios, except for the results obtained at negative load ratios and especially at R =-0.5.

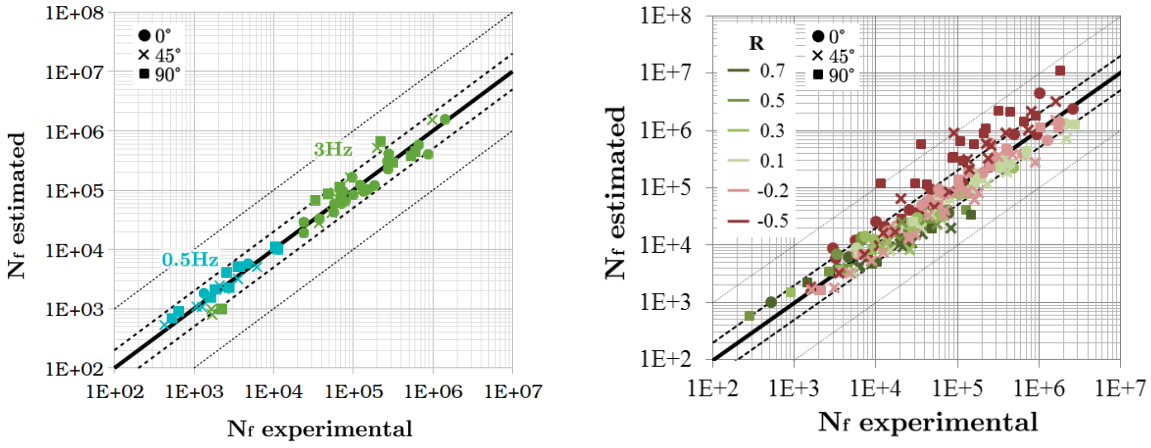

(a) Free convection - f = 0.5-3Hz

(b) Forced convection - f = 3Hz

Figure 14: Estimated fatigue life using eq. (4) vs. experimental number of cycle to failure - RH50 specimens. Scatter bands of factor 2 and 10 are marked in dashed and dotted lines respectively.

4.3. Mixed criterion: anelastic energy and cyclic strain rate

Although yielding very good results for positive load ratios, the cyclic strain rate based criterion presented above is less precise when it comes to negative load ratios. However, we have shown that the anelastic energy W_{an} is a parameter unifying results for these negative load ratios.

We can therefore plot a 3D diagram with the number of cycle to failure versus both the cyclic strain rate and the anelastic energy (fig. 15(a)).

Two regimes can be distinguished:

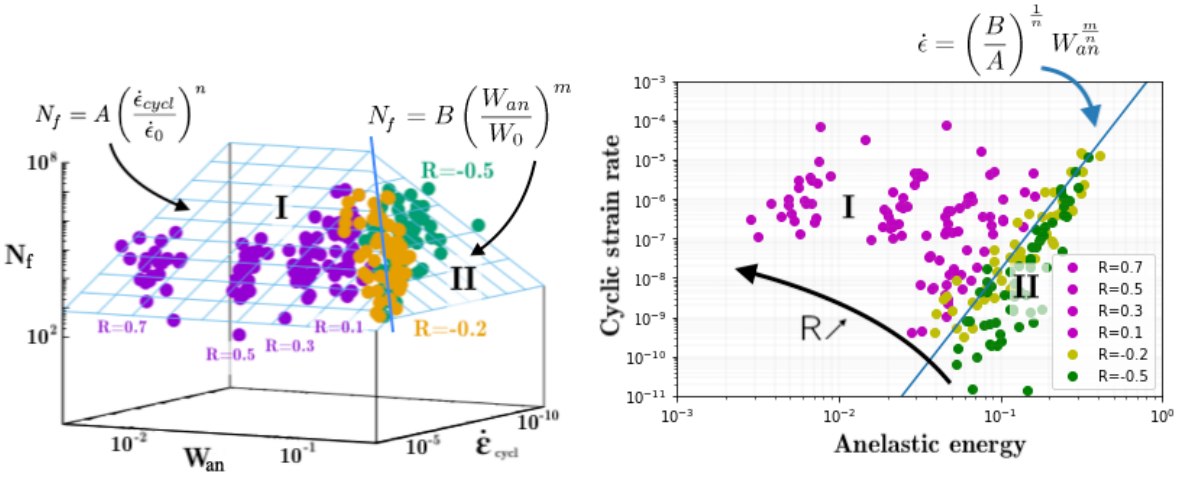

(a) 3D scatter plot of the N_f vs. W_{an} and $\dot{\epsilon}_{cycl}$

(b) $\dot{\epsilon}_{cycl}$ vs. W_{an}

Figure 15: Analysis to establish a relationship between the number of cycle to failure N_f, the anelastic energy W_{an} and the cyclic strain rate $\dot{\epsilon}_{cycl}$ - RH50 specimens - f = 3Hz - forced convection - all fiber orientations.

- for positive load ratios, the durability is mostly driven by the cyclic creep behavior of the material (*i.e.* by the cyclic mean strain rate).
- for negative load ratios, because of the high stress amplitude, the dissipative behavior becomes dominant. The fatigue lifespan is then mostly driven by an energetic parameter.

It is worth noting that the present work deals with positive load ratios up to 0.7. A load ratio equal to 1 would correspond to a static creep test and is not addressed here.

As a first approach we consider each of these regimes to be driven by only one parameter ($\dot{\epsilon}_{cycl}$ or W_{an} respectively). These two regimes are represented by two distinct surfaces in fig. 15(a) defined by:

$$N_f^I = A\left(\frac{\dot{\epsilon}_{cycl}}{\dot{\epsilon}_0}\right)^n \tag{5}$$

$$N_f^{II} = B\left(\frac{W_{an}}{W_0}\right)^m \tag{6}$$

Parameters A and n (resp. B and m) are determined by fitting experimental data for positive (resp. negative) load ratios:

$$A = 1.29 \text{ and } n = -0.674 \text{ for domain I.}$$
$$B = 65.61 \text{ and } m = -3.547 \text{ for domain II.}$$

A trivial, yet effective, approach would consist in estimating the number of cycles to failure as the minimum of eqs. (5) and (6):

$$N_f = \min\left[A\left(\frac{\dot{\epsilon}_{cycl}}{\dot{\epsilon}_0}\right)^n, B\left(\frac{W_{an}}{W_0}\right)^m\right] \tag{7}$$

This yields very good results for all load ratios and fiber orientations (fig. 16), with almost every estimated N_f being within a scatter band of factor 2 around the experimental values.

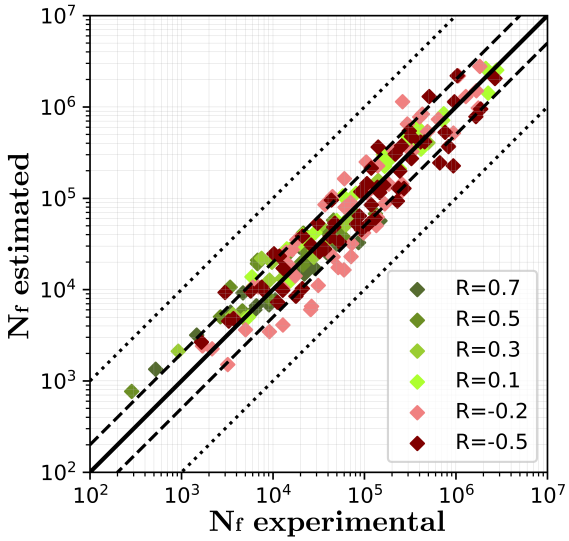

Figure 16: Estimated fatigue life using eq. (7) vs. experimental number of cycle to failure - RH50 specimens - f = 3Hz - forced convection - all fiber orientations. Scatter bands of factor 2 and 10 are marked in dashed and dotted lines respectively.

However it also possible to obtain a *continuous* criterion by using a weight function to ensure the transition between the cyclic creep (I) and the dissipative regime (II).

Let f be the weight function defined by:

$$f = \frac{1}{2}\left\{1 + \tanh[\gamma(\alpha_0 - \alpha(\dot{\epsilon}_{cycl}, W_{an}))]\right\} \tag{8}$$

with $\alpha_0 = \left(\frac{B}{A}\right)^{\frac{1}{n}}$ and:

$$\alpha(\dot{\epsilon}_{cycl}, W_{an}) = \frac{\dot{\epsilon}_{cycl}}{\dot{\epsilon}_0}\left(\frac{W_{an}}{W_0}\right)^{-\frac{m}{n}} \tag{9}$$

The parameter α_0 indicates the boundary between the two regimes as illustrated in fig. 15(b). Values for m and n used in the calculation of α_0 and eq. (9) are subjected to an optimization process, as detailed below.

The parameter γ determines the *sharpness* of the transition between the two regimes (figs. 18(a) and 18(b)). The range for γ was chosen to have two extreme cases: 10 for smooth transition between the two branches of the model while 10^4 provides with a sharp transition (see fig. 17).

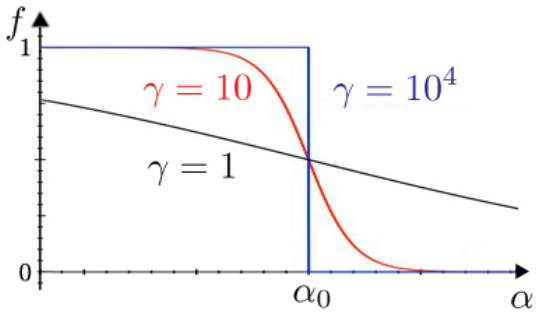

Figure 17: Weight function f for various values of the parameter γ

We can then determine the number of cycles to failure as:

$$N_f = (1 - f) \cdot A \left(\frac{\dot{\epsilon}_{cycl}}{\dot{\epsilon}_0} \right)^n + f \cdot B \left(\frac{W_{an}}{W_0} \right)^m \tag{10}$$

Parameters A, n, B and m are optimized to minimize the discrepancy between the estimated and experimental N_f over the whole dataset. Note that the values of α_0 and α are updated during the optimization process with the correct values of parameters n and m. This yields, for $\gamma = 10^4$:

$$A = 0.851,\ n = -0.660$$
$$B = 123.9,\ m = -3.247$$

For low values of γ (e.g. $\gamma = 10$) not enough correction is applied and the results are not better than with a simple strain rate criterion (eq. (4)). However, larger values (e.g. $\gamma = 10^4$) yield very good results, even at high N_f and for negative load ratios R (fig. 18(d)).

It should also be pointed that instead of being fixed prior to the optimisation of the other parameters, the parameter γ can also be included in the optimization process. Optimized value is $\gamma_{opt} = 54390$, with very little change to the other parameters ($A = 0.838$, $n = -0.661$, $B = 117.8$, $m = -3.263$) and a criterion that only yields minimal improvement as shown in fig. 19.

4.4. Identification on a smaller database

The criteria presented above (eq. (10)) has been identified on results from 207 fatigue tests. If a similar criterion was to be applied for a new material, obtaining such a large experimental database would be long and costly. The question thus arises of the accuracy of a criterion identified on a smaller set of experimental results.

In order to give an insight on these possibilities, various datasets for identification have been tested. Figure 19 gives the relative error made on the estimation of N_f based on the following datasets:

- Separate: all 207 specimens were used with parameters identified separately for each of the two regimes. Similar as obtained by eq. (7) and plotted on fig. 16.

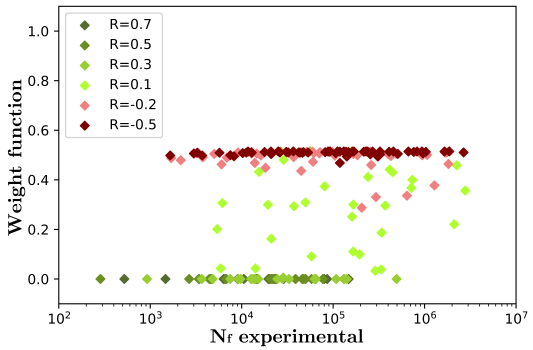

(a) Weight function vs. N_f - $\gamma = 10$

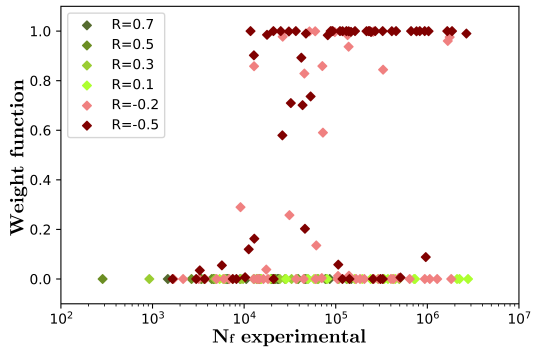

(b) Weight function vs. N_f - $\gamma = 10^4$

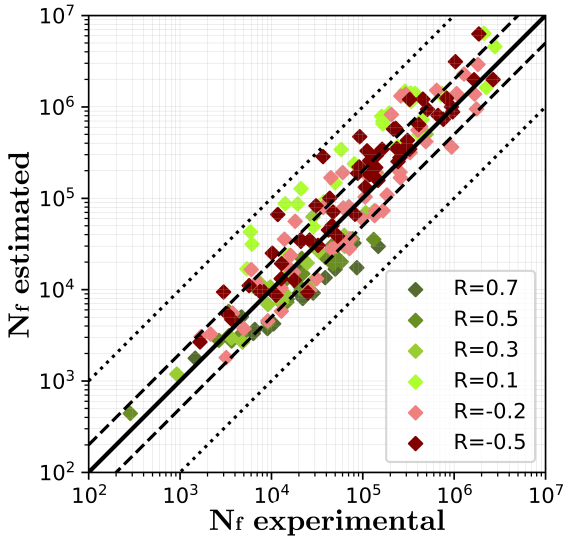

(c) Estimated fatigue life with $\gamma = 10$ vs. experimental number of cycles to failure

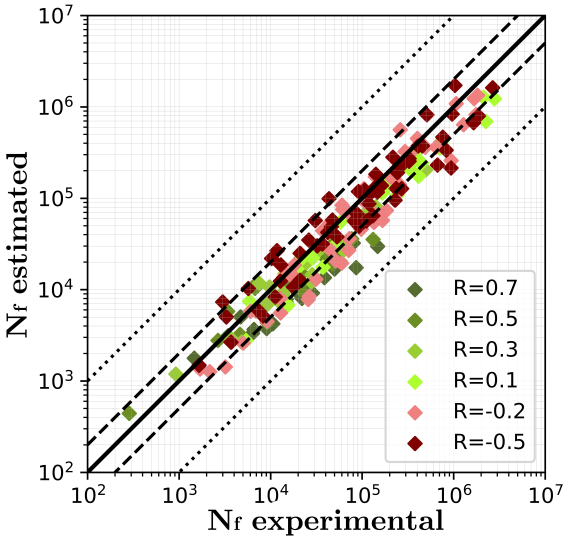

(d) Estimated fatigue life with $\gamma = 10^4$ vs. experimental number of cycles to failure

Figure 18: Weight function f and estimated fatigue life using the mixed criterion [eq. (10)] for all fiber orientations. Scatter bands of factor 2 and 10 are marked in dashed and dotted lines respectively.

- 0° - $\gamma = 10^4$: only results on 0° specimens were used for identification - 66 specimens in total. Value of γ was set to 10^4.
- All spc - $\gamma = 10$: all 207 specimens were used with parameters identified over the whole dataset. Value of γ was set to 10. Corresponds to results given on fig. 18(c).
- 27 spc - $\gamma = 10^4$: only 3 specimens per orientation (0°, 45°, 90°) for only three of the load ratios (R=$[-0.5; 0.1; 0.7]$) were used for identification - 27 specimens in total. For each configuration, the 3 specimens were chosen with N_f values around 10^3, 10^4, and 10^5 or above, to cover over the whole range of fatigue lives. Value of γ was set to 10^4.
- 106 spc - $\gamma = 10^4$: only specimens for three of the load ratios (R=$[-0.5; 0.1; 0.7]$) were used for identification - 106 specimens in total. Value of γ was set to 10^4.
- All spc - $\gamma = 10^4$: all 207 specimens were used with parameters identified over the whole dataset. Value of γ was set to 10^4. Corresponds to results given on fig. 18(d).
- All spc - $\gamma = 54390$: all 207 specimens were used with parameters identified over the whole dataset. Value of γ was also set as an optimization variable, yielding $\gamma = 54390$.

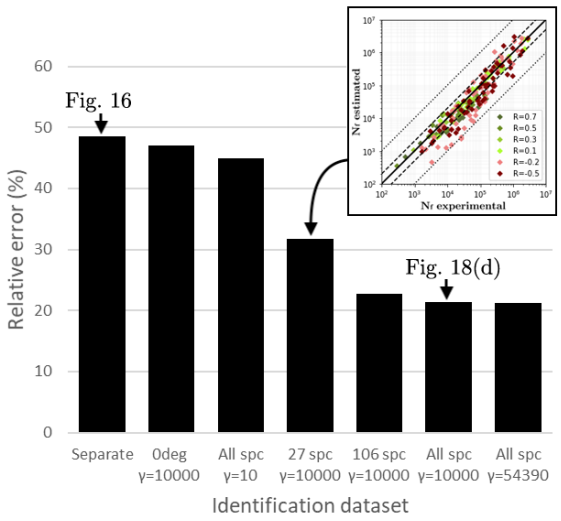

Figure 19: Relative error on N_f using the mixed criterion eq. (10) identified on various datasets.

Note that a relative error of 50% might seem important, but is in fact already very small compared to the usual fatigue predictions often spanning more than a decade.

Even though more analysis would be required to determine the minimal necessary experimental dataset to obtain the desired accuracy of the identified criterion, fig. 19 shows that relatively good results can be obtained with only a very reduced number of specimens compared to the 207 included in this study.

5. Conclusion

Fatigue testing was performed on specimens with multiple fiber orientations. Several mechanical parameters were analyzed in order to determine a relevant indicator for durability estimation. We showed that a simple two parameters strain-rate based criterion was very effective in unifying fatigue results for positive load ratios.

In our case, so as to further improve the prediction for all load ratios, a second criterion was introduced, allowing to take into account the dissipative behavior of the material under high stress amplitudes. This criterion yields particularly good results when compared to experimental data.

Several outlooks can be considered. First, as the fatigue criterion was established for smooth specimens under uniaxial loadings, the focus should now be set on notched specimens and multiaxial loadings. In these cases the use of an equivalent strain measurement and/or non-local criterion might be required.

Second, in the mixed criterion introduced in the present work two regimes were used. Although damage mechanisms for the cyclic creep regime (I) are now well understood [22, 23], it would be interesting to study damage mechanisms in the dissipative regime (II). This would further support the use of a mixed - two mechanisms criterion.

Finally by considering the cyclic strain rate at mid-life we show the possibility of estimating the fatigue life without exhausting all the cycles. However, deeper study of the cyclic strain rate evolution during fatigue loading should be performed.

This might allow for a similar criterion to be based on the initial evolution of the cyclic strain rate, making it of more practical use for industrial applications on complex parts by avoiding time consuming computations. Moreover the development of skip cycle methodologies for strongly non linear constitutive models may be of particular usage.

Acknowledgements

The authors gratefully acknowledge Solvay Performance Polyamides for supporting this work and for providing specimens.

This work was partly performed in the framework of the DURAFIP project (FUI project supported by Oseo). Authors would also like to thank the ANRT (French National Association for Research and Technology) for its financial support via a CIFRE grant.

References

[1] Seyyedvahid Mortazavian and Ali Fatemi. Fatigue behavior and modeling of short fiber reinforced polymer composites: A literature review. *International Journal of Fatigue*, 70:297–321, 2015.

[2] J. J. Horst. *Influence of fibre orientation on fatigue of short glassfibre reinforced Polyamide*. PhD thesis, TU Delft, 1997.

[3] A. Bernasconi and R. M. Kulin. Effect of Frequency Upon Fatigue Strength of a Short Glass Fiber Reinforced Polyamide 6: A Superposition Method Based on Cyclic Creep Parameters. *Polymers and Polymer Composites*, 2009.

[4] Mohammadreza Eftekhari and Ali Fatemi. On the strengthening effect of increasing cycling frequency on fatigue behavior of some polymers and their composites: Experiments and modeling. *International Journal of Fatigue*, 87:153–166, 2016.

[5] Muhamad Fatikul Arif. *Damage mechanisms in short glass fiber reinforced polyamide-66 under monotonic and fatigue loading : Effect of relative humidity and injection molding induced microstructure.* PhD thesis, ENSAM, 2014.

[6] A. Bernasconi, F. Cosmi, and E. Zappa. Combined effect of notches and fibre orientation on fatigue behaviour of short fibre reinforced polyamide. *Strain*, 46(5):435–445, 2010.

[7] Ali Fatemi, Seyyedvahid Mortazavian, and Abolhasan Khosrovaneh. Fatigue Behavior and Predictive Modeling of Short Fiber Thermoplastic Composites. *Procedia Engineering*, 133:5–20, 2015.

[8] P. K. Mallick and Yuanxin Zhou. Effect of mean stress on the stress-controlled fatigue of a short E-glass fiber reinforced polyamide-6,6. *International Journal of Fatigue*, 26(9):941–946, 2004.

[9] Hideki Oka, Ryoichi Narita, Yoshiaki Akiniwa, and Keisuke Tanaka. Effect of Mean Stress on Fatigue Strength of Short Glass Fiber Reinforced Polybuthyleneterephthalate. *Key Engineering Materials Vols.*, 341:537–542, 2007.

[10] Mohammadreza Eftekhari and Ali Fatemi. Creep-fatigue interaction and thermomechanical fatigue behaviors of thermoplastics and their composites. *International Journal of Fatigue*, 91:136–148, 2016.

[11] Elodie Mourglia Seignobos. *Compréhension des mécanismes physiques de fatigue dans le polyamide vierge et renforcé de fibres de verre.* PhD thesis, INSA Lyon, 2009.

[12] E. C. Monkman and N. J. Grant. An empirical relationship between rupture life and minimum creep rate in creep– rupture test. *Proc. Am. Soc. Test. Mater.*, page 593, 1956.

[13] A. Bernasconi, F. Cosmi, and D. Dreossi. Local anisotropy analysis of injection moulded fibre reinforced polymer composites. *Composites Science and Technology*, 68(12):2574–2581, 2008.

[14] Abderrahmane Ayadi, Hedi Nouri, Sofiane Guessasma, and Frederic Roger. Determination of orthotropic properties of glass fibre reinforced thermoplastics using X-ray tomography and multiscale finite element computation. *Composite Structures*, 136:635–649, 2016.

[15] Héloïse Rolland. *Comportement en fatigue et mécanismes d'endommagement du polyamide 6,6 renforcé de fibres courtes.* PhD thesis, ENSAM, 2017.

[16] E. Macha and C. M. Sonsino. Energy criteria of multiaxial fatigue failure. *Fatigue and Fracture of Engineering Materials and Structures*, 22(12):1053–1070, 1999.

[17] Adil Benaarbia. *Analyse énergétique du comportement thermomécanique du PA6.6 renforcé de fibres de verre*. PhD thesis, Université Montpellier 2, 2014.

[18] Adil Benaarbia, André Chrysochoos, and Gilles Robert. Thermomechanical behavior of PA6.6 composites subjected to low cycle fatigue. *Composites Part B: Engineering*, 76:52–64, 2015.

[19] Nicolas Saintier, Thierry Palin-Luc, Jérôme Bénabes, and Francis Cocheteux. Non-local energy based fatigue life calculation method under multiaxial variable amplitude loadings. *International Journal of Fatigue*, 54:68–83, 2013.

[20] A. Bernasconi, P. Davoli, A. Basile, and A. Filippi. Effect of fibre orientation on the fatigue behaviour of a short glass fibre reinforced polyamide-6. *International Journal of Fatigue*, 29(2):199–208, 2007.

[21] A. M. Vinogradov and S. Schumacher. Cyclic creep of polymers and polymer-matrix composites. *Mechanics of Composite Materials*, 37(1):29–34, 2001.

[22] I Raphael, N Saintier, G Robert, J Béga, and L Laiarinandrasana. On the role of the spherulitic microstructure in fatigue damage of pure polymer and glass-fiber reinforced semi-crystalline polyamide 6.6. *International Journal of Fatigue*, 126:44–54, 2019.

[23] H Rolland, N Saintier, I Raphael, N Lenoir, A King, and G Robert. In-situ fatigue damage mechanisms in short fibre reinforced PA66 as observed by synchrotron X-ray microtomography. *Composites Part B: Engineering*, 143(December 2017):217–229, 2018.